Title
Biome-specific scaling of ocean productivity, temperature, and carbon export efficiency

Journal
Geophysical Research Letters, 43(10)

ISSN
0094-8276

Authors
Britten, Gregory L
Primeau, François W

Publication Date
2016-05-28

DOI
10.1002/2016gl068778

AGU PUBLICATIONS

Geophysical Research Letters

RESEARCH LETTER
10.1002/2016GL068778

Key Points:
- Optimized models predict carbon export efficiency from net primary production and sea surface temperature
- Biome-specific relationships impact global export inferred from satellite-derived variables
- Individual biomes respond differently to simulated net primary production and sea surface temperature changes

Supporting Information:
- Supporting Information S1
- Data Set S1
- Data Set S2

Correspondence to:
G. L. Britten,
gbritten@uci.edu

Citation:
Britten, G. L., and F. W. Primeau (2016), Biome-specific scaling of ocean productivity, temperature, and carbon export efficiency, *Geophys. Res. Lett.*, *43*, 5210–5216, doi:10.1002/2016GL068778.

Received 21 MAR 2016
Accepted 29 APR 2016
Accepted article online 2 MAY 2016
Published online 24 MAY 2016

Biome-specific scaling of ocean productivity, temperature, and carbon export efficiency

Gregory L. Britten[1] and François W. Primeau[1]

[1]Department of Earth System Science, University of California, Irvine, USA

Abstract Mass conservation and metabolic theory place constraints on how marine export production (EP) scales with net primary productivity (NPP) and sea surface temperature (SST); however, little is empirically known about how these relationships vary across ecologically distinct ocean biomes. Here we compiled in situ observations of EP, NPP, and SST and used statistical model selection theory to demonstrate significant biome-specific scaling relationships among these variables. Multiple statistically similar models yield a threefold variation in the globally integrated carbon flux (~4–12 Pg C yr^{-1}) when applied to climatological satellite-derived NPP and SST. Simulated NPP and SST input variables from a 4×CO_2 climate model experiment further show that biome-specific scaling alters the predicted response of EP to simulated increases of atmospheric CO_2. These results highlight the need to better understand distinct pathways of carbon export across unique ecological biomes and may help guide proposed efforts for in situ observations of the ocean carbon cycle.

1. Introduction

Ocean biology plays a significant role in the global carbon cycle by exporting organic carbon to deep waters where it is remineralized back to CO_2 and may remain sequestered for timescales of tens to thousands of years [*Kwon et al.*, 2009; *DeVries et al.*, 2012]. However, ocean regions are characterized by unique ecological biomes with variable ecosystem structure that exhibit distinct pathways of carbon uptake, trophic transfer, and remineralization [*DeVries and Deutsch*, 2014; *Teng et al.*, 2014; *Henson et al.*, 2015] and likely respond differently to climate-driven changes in temperature and primary productivity. Satellite-derived oceanic net primary productivity (NPP) and sea surface temperature (SST, here used as a proxy for euphotic zone temperature) are thought to provide a basis to infer oceanic carbon export at global scales [*Dunne et al.*, 2005; *Henson et al.*, 2011; *Laws et al.*, 2011; *Siegel et al.*, 2014], yet the relationships used for global extrapolation remain uncertain, and very little is known about how the functional form and/or rate parameters vary across unique biomes and ecosystem types [*Henson et al.*, 2015]. Cost and logistical difficulty has limited the observational basis from which to study and extrapolate biome-specific variability to the global scale. An upcoming 5 year NASA study [*Siegel et al.*, 2015] aims to address this uncertainty with increased field-based carbon export sampling. Here we adopt a statistical approach to evaluate current evidence for biome-specific drivers of export by synthesizing available in situ observations of NPP, SST, and EP and using model selection theory to determine whether these relationships depend on ecosystem type. We then investigate the spatial pattern of these relationships and evaluate the consequences for global extrapolation of export flux based on NPP and SST.

The most common empirical models of carbon export parameterize the fraction of NPP exported (*ef*) as an increasing function of NPP and a decreasing function of SST [*Laws et al.*, 2000, 2011; *Dunne et al.*, 2005; *Henson et al.*, 2011]. Ecological theory states that heterotrophic respiration temporally lags autotrophic production such that an increasing fraction of NPP can be exported at high productivity by way of sinking particles [*Sarmiento and Gruber*, 2013]. The SST effect, however, negatively scales EP by increasing the rate of respiratory biochemical reactions more quickly than autotrophic reactions such that the ratio of autotrophic production to heterotrophic metabolism declines as temperature increases [*López-Urrutia et al.*, 2006], leading to lower EP at high SST. A variety of scaling models that predict *ef* as a function of NPP and SST, denoted here *ef*(NPP, SST), have been developed to extrapolate global EP from satellite-derived NPP and SST [*Laws et al.*, 2000, 2011; *Dunne et al.*, 2005; *Henson et al.*, 2011] and thus provide a relatively simple means to predict and monitor key ocean carbon cycle processes from space. These models have also been used as simplified "subecosystem scale parameterizations" [*Galbraith et al.*, 2015] of carbon cycling processes within larger biogeochemical and climate models [*Bopp et al.*, 2001; *Deutsch et al.*, 2007] as well as in food web models for fisheries [*Friedland et al.*, 2012], demonstrating the wide utility of *ef*(NPP, SST) relationships.

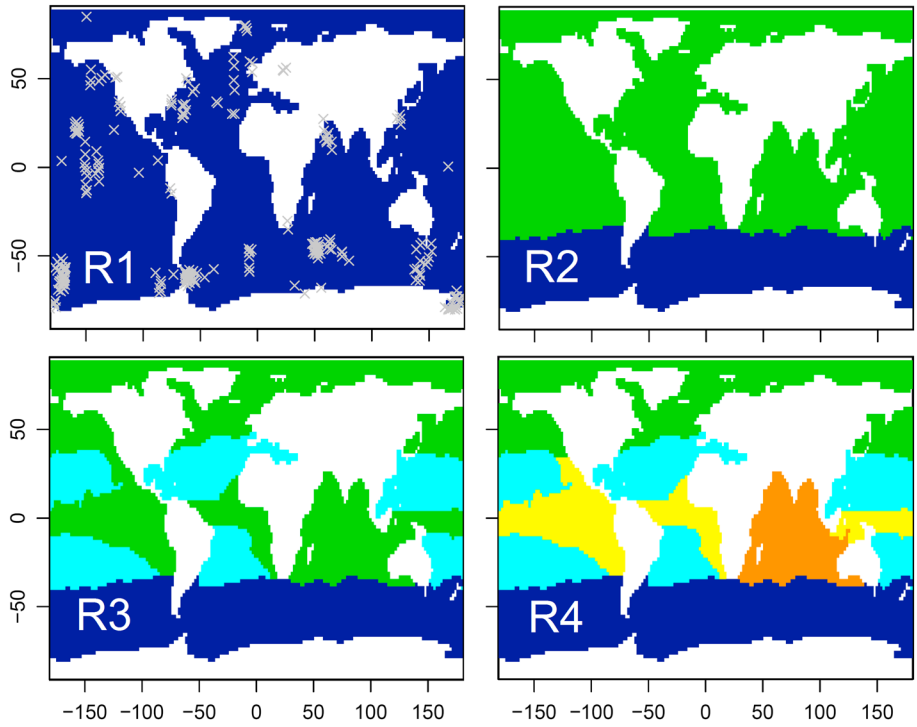

Figure 1. Location of observations and biome configurations tested within the model selection framework. Biome definitions R1–R4 are generalized versions of those defined in *DeVries and Deutsch* [2014] and *Teng et al.* [2014], based on nutrient concentration, remineralization, and light availability.

The simplest and most commonly used *ef*(NPP, SST) scaling models take the form of three-parameter functional response curves

[*Laws et al.*, 2011]
$$ef(\mathrm{NPP}, \mathrm{SST}) = \frac{(a - b\mathrm{SST})\mathrm{NPP}}{\mathrm{NPP} + c}, \quad (1)$$

[*Laws et al.*, 2011]
$$ef(\mathrm{NPP}, \mathrm{SST}) = (a - b\mathrm{SST})\mathrm{NPP}^c, \quad (2)$$

[*Dunne et al.*, 2005]
$$ef(\mathrm{NPP}, \mathrm{SST}) = a\log\left(\frac{\mathrm{NPP}}{Z}\right) - b\mathrm{SST} + \mathrm{c}, \quad (3)$$

where a, b, and c are empirically estimated parameters and Z is the depth of the euphotic zone. Until recently, *ef*(NPP, SST) parameters have been assumed globally constant; however, recent empirical [*Maiti et al.*, 2013; *Martin et al.*, 2013; *Laurenceau-Cornec et al.*, 2015] and modeling [*Henson et al.*, 2015] evidence suggest that temperature and productivity may affect *ef* in ways that are strongly dependent on regional ecosystem structure and dynamics. For example, several studies have recently documented an inverse relation between *ef* and NPP in the Southern Ocean [*Maiti et al.*, 2013; *Martin et al.*, 2013; *Laurenceau-Cornec et al.*, 2015], possibly related to unique interactions among silica limitation, sinking speed, and low SST regimes [*Henson et al.*, 2015]. Furthermore, it is well known that biological metabolism follows a nonlinear relationship with temperature [*Gillooly et al.*, 2001; *López-Urrutia et al.*, 2006] whereby the relative effect of temperature is predicted to be strongest in low-temperature regimes and weakest at high-temperature regimes. While these complications have been recently highlighted as potentially important at the global scale [*López-Urrutia et al.*, 2006; *Henson et al.*, 2015], it is yet unknown how *ef*(NPP, SST) scaling varies across distinct ecosystem types in terms of functional form and spatial parameter variability. Consequently, it is also unknown how variable scaling relationships may alter satellite-derived global carbon cycle predictions and how carbon cycling in distinct ocean biomes may respond to future changes in temperature and primary productivity.

Here we help address these uncertainties by compiling available in situ observations of NPP, SST, and EP. We then use ocean biome configurations that separate the ocean into distinct regions based on nutrient concentration, elemental remineralization ratios, and light availability. We test for significant biome-specific scaling by allowing the parameters of equations (1)–(3) to vary across each biome configuration shown in Figure 1 and then determine the best fitting biome configuration according to statistical model selection (described in section 2). We then evaluate the impact of biome-specific scaling on globally integrated export production by extrapolating biome-specific models to the global scale with satellite-derived climatological fields of NPP and SST. Finally, to demonstrate how the estimated biome-specific *ef*(NPP, SST) scaling may affect the response of the marine carbon cycle to climate change, we evaluate biome-specific changes in EP in a simulated high CO_2 world scenario using NPP and SST inputs from the Geophysical Fluid Dynamics Laboratory (GFDL) ESM Earth System Model in a 4×CO_2 experiment.

2. Materials and Methods

2.1. Data Sources

The in situ observations of EP, NPP, and SST were compiled from the data collections published in *Laws et al*. [2000], *Dunne et al*. [2005, 2007], and *Maiti et al*. [2013]. After removing duplicates, the database contains 274 unique in situ observations. The measurement techniques of EP come primarily from sediment trap-based measurements and the 234-Thorium method, while NPP was primary measured through the ^{14}C method. A 10 year annual climatology (years 2002–2012) of satellite-based NPP was constructed from monthly NPP data products downloaded from http://www.science.oregonstate.edu/ocean.productivity according to the carbon-based productivity model [*Westberry et al*., 2008]. For satellite-based SST, the same 10 year (2002–2012) mean annual SST climatology was computed from daily SST observations extracted from http://data.nodc.noaa.gov/pathfinder. Ten-year climatological euphotic zone depth (1997–2007) was downloaded from http://oceancolor.gsfc.nasa.gov/ based on SeaWiFs data and the algorithm described in *Lee et al*. [2007]. To evaluate the consequences of biome-specific relationships for climate change, predictions for future SST and NPP under a 4×CO_2 climate model experiment were downloaded from the GFDL ESM2 Earth System Model database (http://data1.gfdl.noaa.gov/). The model experiment is part of the CMIP5 climate model ensemble whereby atmospheric CO_2 is prescribed to increased by 1% per year from a preindustrial state until reaching 4 times the preindustrial CO_2 (i.e. a preindustrial atmosphere of 285 ppm increases at 1% per year until it reaches 1140 ppm in 140 model years).

2.2. Model Fitting and Statistical Model Selection

The model fitting and selection is performed to test how the numerical parameters of equations (1)–(3) may vary across the ocean biome definitions presented in Figure 1. We test four ocean biome configurations of increasing complexity and number of adjustable parameters: (1) globally fixed (denoted R1), (2) distinct Southern Ocean parameters (R2), (3) distinct Southern Ocean and subtropical gyres (R3), and (4) distinct Southern Ocean, subtropical gyres, equatorial upwelling, and Indian Ocean (R4).

For any one particular biome configuration we estimated the parameters of equations (1)–(3) using the method of maximum likelihood assuming Gaussian-distributed model errors. We combine the likelihoods from each biome by summing the log likelihood

$$\mathrm{ll}(f,\boldsymbol{\theta}) = \Sigma_i \mathrm{ll}(\boldsymbol{\theta}_i) = -\Sigma_i \frac{n_i}{2}\ln(2\pi) - \frac{n_i}{2}\ln\left(\sigma_i^2\right) - \frac{1}{2\sigma_i^2}\left|\mathbf{EF}_i - f(\boldsymbol{\theta}_i)\right|^2,$$

where ll represents the log likelihood for functional form f parameterized by parameter vector $\boldsymbol{\theta}$. The subscript i identifies an individual biome with biome-specific parameters $\boldsymbol{\theta}_i$, where $\mathbf{EF}_i$ represents the vector of observed export fractions, n_i represents the number of observations, and the residual error variance is σ_i^2. For each biome configuration (R1–R4) and each functional form (equations (1)–(3)) we numerically optimize ll (f, $\boldsymbol{\theta}$) with respect to $\boldsymbol{\theta}$ to obtain the maximum likelihood estimates for the model parameters, denoted $\widehat{\boldsymbol{\theta}}$. The increasing complexity and nested structure of the four configurations means that the log likelihood (and many other goodness of fit diagnostics such as R^2) can only improve as we increase biome complexity from configuration R1 to configuration R4. We therefore utilize the Bayesian Information Criterion (BIC) [*Kass and*

Raftery, 1995] to balance goodness of fit against model complexity (number of adjustable parameters) and avoid overfitting. The BIC is defined as

$$\mathrm{BIC} = \mathrm{ll}\left(\hat{\boldsymbol{\theta}}\right) - k\log(n),$$

where $\mathrm{ll}\left(\hat{\boldsymbol{\theta}}\right)$ is the log likelihood evaluated at the maximum likelihood estimates, k is the length of the parameter vector (note that each biome has parameters a, b, c, and residual error variance σ^2; therefore, k equals 4 times the number of biomes), and n is total number of observations in the database. The formula for the BIC arises as a simple and readily calculable approximation to the log of the Bayesian model evidence [*Kass and Raftery*, 1995], which represents the probability of the data, given a particular model, after integrating over the uncertainty in the model parameters. According to this approximation, the best fitting model is the one that maximizes the BIC, where the term $k\log(n)$ serves as a penalty for model complexity and sets that the magnitude $\mathrm{ll}\left(\hat{\boldsymbol{\theta}}\right)$ must increase to justify an additional parameter in the model. To compare models of variable biome complexity, we compute the difference in the BIC among different biome configurations and functional forms

$$\Delta\mathrm{BIC} = \max(\mathrm{BIC}) - \mathrm{BIC}_R$$

where BIC_R is the optimized BIC for each biome configuration of a particular functional form and max(BIC) is the BIC from the best fitting biome configuration for that functional form. The ΔBIC is used for model selection because it approximates the log of the Bayes factor (or the ratio of model evidences) according to $\Delta\mathrm{BIC} \approx 2\log(p_i/p_j)$ where p_i/p_j is the fitted odds of biome configuration i over j. The magnitude of the ΔBIC therefore measures the strength of empirical evidence for one biome configuration over another while taking into account the additional number of parameters required to fit more complex configurations. For example, a ΔBIC of 6 would represent approximately 20:1 odds for biome configuration i over biome configuration j which is roughly analogous to an $\alpha = 0.05$ classical significance test. The reader is referred to *Kass and Raftery* [1995] and *Burnham and Anderson* [2002] for comprehensive discussions of ΔBIC-based model selection.

3. Results and Discussion

We found strong statistical support for biome-specific *ef*(NPP, SST) scaling (Figures 2 (left) and 3) whereby all three functional forms indicated that the added complexity of biome-specific models could be justified based on the information in the available data. Across all three functional forms, globally fixed parameters yielded ΔBIC values >50, which indicates negligible statistical support for globally constant configurations. The best fitting biome configuration was the R3 biome configuration, indicating significantly different parameters for the Southern Ocean and the subtropical gyres, relative to the rest of the ocean. However, a total of eight additional model configurations (R3 and R4 for equation (1) and R2, R3, and R4 for equations (2) and (3)) gave $\Delta\mathrm{BIC} < 7$, relative to the best fitting R3 biome configuration, indicating relatively weak statistical separation despite large variation in model complexity (Table S1 in the supporting information). This result indicates that the in situ database strongly supports biome-specific scaling but provides insufficient information to distinguish the specific pattern of parameter variability across ocean biomes. Optimized parameters, their uncertainty, and a graphical display of fitted *ef*(NPP, SST) are given for all model fits in the supporting information, along with their associated BIC and R^2 diagnostics.

We also found that biome-specific scaling has strong implications for satellite-based extrapolation of global EP (Figures 2 (right) and S1a). Using the climatological, annually averaged satellite-derived NPP and SST, globally integrated EP for R2, R3, and R4 configurations gave predicted values of approximately 11.5, 5, and 7 Pg C yr^{-1}, respectively, with $<10\%$ relative variation across functional forms. The weak resolution, yet significant impact of biome-specific *ef*(NPP, SST), therefore limits our ability to monitor and accurately infer global EP using the type of empirical models discussed here. This inaccuracy may have consequences for a variety of studies that incorporate *ef*(NPP, SST) relationships into larger models and calculations.

The inferred biome-specific *ef*(NPP, SST) scaling showed marked variability relative to globally fixed relationships, particularly in terms of the Southern Ocean productivity effect and the role of temperature (Figure 3). The Southern Ocean productivity relationship strongly reflects that demonstrated by *Maiti et al*. [2013], having incorporated those data in this analysis. The results here therefore support [*Maiti et al*., 2013] and also

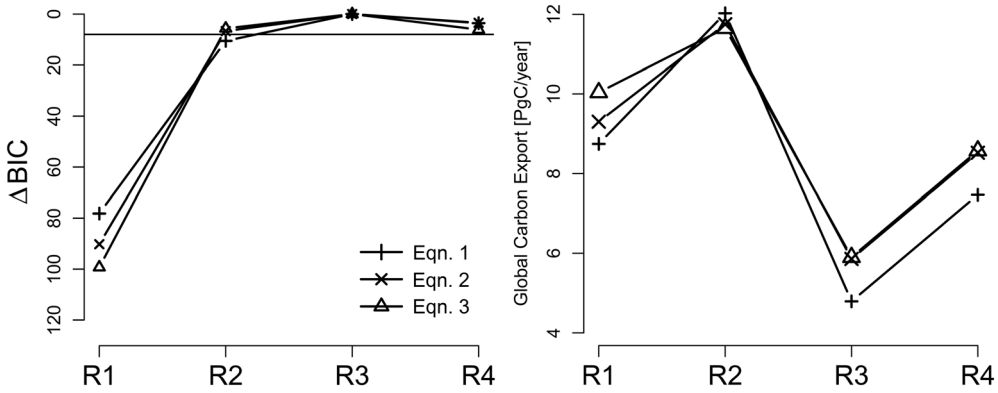

Figure 2. (left) Model selection results and (right) satellite-based globally extrapolated carbon export predictions based on various functional forms (equations (1)–(3)) and biome-specific *ef*(NPP, SST) scaling parameters.

further identify the uniqueness of the inverse Southern Ocean productivity relationship in the context of a larger global data set. Under the R4 biome configuration, the Northern Ocean (NO) biome (which represents the Arctic Ocean and the northern regions of the Atlantic and Pacific Oceans) also showed an inverse relation between export efficiency and NPP (Figure S2c); however, the optimized parameters were highly uncertain and indistinguishable from zero due to a low number of observations across the Northern Ocean biome ($n = 22$). The inferred *ef*(NPP, SST) relationships for the subtropical gyres and the rest of the ocean are similar to one another in their strong positive NPP effect but differed in magnitude for the SST effect (Figure 3). The SST effect was found to be relatively weak in the subtropical gyres relative to the rest of the ocean, which is consistent with metabolic theory [*López-Urrutia et al*., 2006] that predicts the weakest temperature effect in high-temperature regimes).

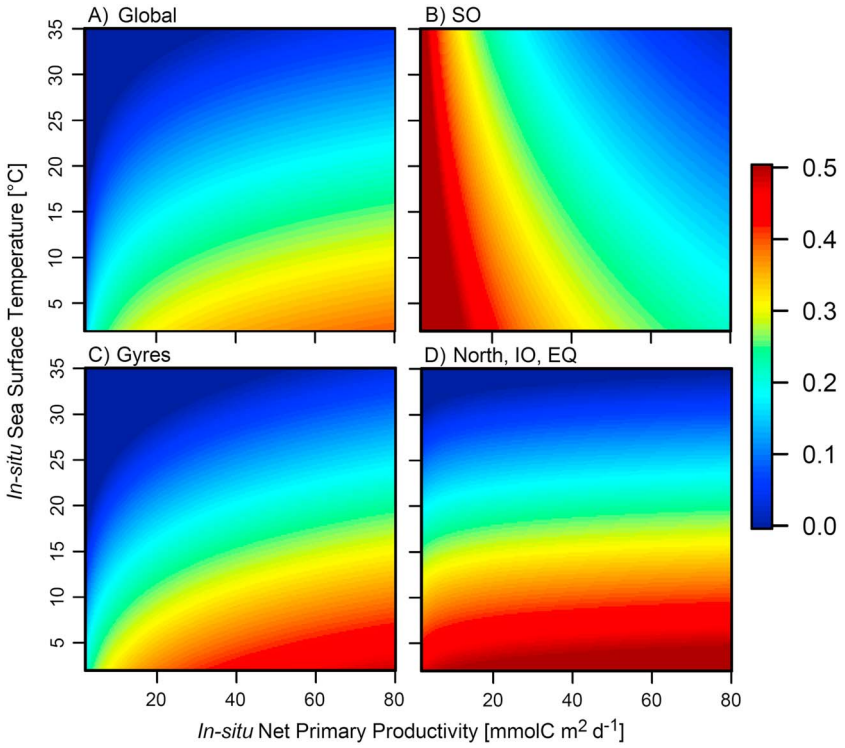

Figure 3. Inferred biome-specific *ef*(NPP, SST) scaling relationships based on the best fitting R3 biome configuration and the power law parameterization (equation (2)). (a) The globally fixed relationship from equation (2) presented by *Laws et al*. [2011] and (b–d) the biome-specific relationships inferred in this study. The color bar gives the predicted *ef*.

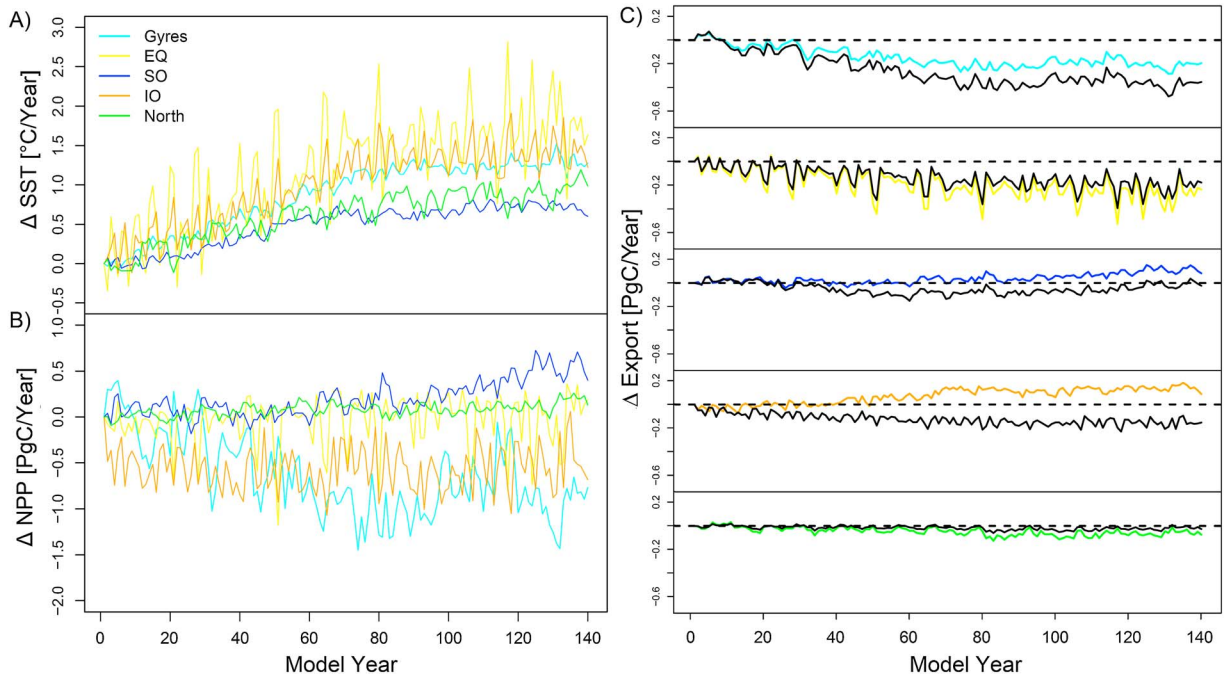

Figure 4. Biome-specific climate change projections for (a) SST and (b) NPP predicted from the GFDL ESM Earth System Model 4×CO_2 climate change experiment. (c) The predicted EP response for the best fitting biome-specific model (colored line) relative to the globally fixed relationships from equation (2) (black line). "Gyres" represents the subtropical gyres, EQ is the equatorial upwelling regions, SO is the Southern Ocean, IO is the Indian Ocean, and NO is the northern region.

Spatial disaggregation of intermodel variability indicated that the subtropical gyre and Indian Ocean biomes yield the greatest range in their contribution to global export estimates. We found that the difference between global and biome-specific scaling was largest for the subtropical gyre biome, where integrated export across the whole biome was nearly half that predicted using globally fixed parameters (Figure S1a). Large areas within both the subtropical gyre and Indian Ocean biomes yielded intermodel variation of >100% across the suite of statistically similar biome configurations (Figure S1b). Large biome-specific variability is likely caused by poor data coverage across large ocean regions (e.g., all Indian Ocean observations are concentrated in the Arabian Sea). The consequent uncertainty in global-scale satellite-based models therefore points to the need for continuing in situ ocean carbon observing at a global scale. A proposed 5 year NASA field sampling program is planned for 2017 [*Siegel et al.*, 2015], aimed specifically at resolving distinct carbon export processes across ecosystem types. The sampling program concentrates observations at two sites: Ocean Station P located in the subarctic North Pacific and the North Atlantic Bloom Experiment site located in the subarctic northeast Atlantic. While these sites provide a unique ecological contrast between the highly seasonal bloom in the North Atlantic and the relatively stable oligotrophic dynamics in the North Pacific, our results point to other regions, such as the subtropical gyre ecosystems and the Indian Ocean, as sites of concentrated uncertainty in satellite-extrapolated predictions of EP from NPP and SST. This empirical modeling framework may therefore help in locating future in situ carbon export observing sites; for example, by performing statistical observing system simulation experiments to determine the areas where future observations would best constrain satellite-based prediction.

Using data from a 4×CO2 climate experiment from the GFDL ESM2 Earth System Model, we also investigated the degree to which biome-specific temperature and productivity scaling impacts the response of carbon export to future climate change (Figures 4a and 4b). Relative to the globally fixed model, we found that the best fitting biome-specific model (equation (2) with R3 biome configuration) predicted weaker EP declines in the gyres (due to the weaker temperature effect in the gyres, consistent with metabolic theory [*López-Urrutia et al.*, 2006]), stronger EP declines in the equatorial and northern biomes, and a sign change from negative to positive in the Southern and Indian Oceans (Figure 3c). By the end of the 4×CO_2 simulation, global export declined by nearly 10% in the globally constant model, whereas the biome-specific model predicts less than 2% change due to partial offsets provided by export increases in the Southern and Indian

Oceans. The total absolute difference in export between the two models at the end of the simulation was nearly 1 Pg C/yr or approximately 10% of current anthropogenic carbon emissions. While these calculations are highly simplified relative to predictions from coupled biogeochemical ocean models, the results highlight the potential importance of biome-specific scaling for the global carbon cycle and also suggest its potential role in determining the ocean's response to ongoing CO_2 emissions. The large uncertainty of these calculations amplifies the need for additional carbon export field sampling in order to observationally constrain biome-specific relationships.

4. Conclusions

In conclusion, distinct biome-specific *ef*(NPP, SST) scaling is predicted to have strong consequences for the response of carbon export to climate change and for satellite-based export estimates. Empirical evidence strongly suggests that export across large ocean regions (e.g., Southern Ocean and subtropical gyres) may uniquely respond to changes in temperature and productivity, while other regions remain unconstrained due to poor observational coverage. Continued observing efforts are needed to resolve these empirical patterns and thereby reduce uncertainty in the global carbon budget and improve carbon cycle monitoring from satellite-based platforms.

Acknowledgments
We acknowledge all the scientists who performed the field studies that contributed to this data synthesis. We also thank the authors of the previous data compilation studies that we synthesized here. Funding for this study was provided by NSF award OCE 1436922. The data synthesis analyzed here can be found as supporting information of this article, along with the spatial masks used to define the biome regions.

References

Bopp, L., P. Monfray, O. Aumont, J.-L. Dufresne, H. Le Treut, G. Madec, L. Terray, and J. C. Orr (2001), Potential impact of climate change on marine export production, *Global Biogeochem. Cycles*, *15*(1), 81–99, doi:10.1029/1999GB001256.

Burnham, K. P., and D. R. Anderson (2002), *Model Selection and Multimodel Inference: A Practical Information-Theoretic Approach*, 2nd ed., Springer-Verlag, New York.

Deutsch, C., J. L. Sarmiento, D. M. Sigman, N. Gruber, and J. P. Dunne (2007), Spatial coupling of nitrogen inputs and losses in the ocean, *Nature*, *445*(7124), 163–167.

DeVries, T., and C. Deutsch (2014), Large-scale variations in the stoichiometry of marine organic matter respiration, *Nat. Geosci.*, *7*(1), 890–894.

DeVries, T., F. Primeau, and C. Deutsch (2012), The sequestration efficiency of the biological pump, *Geophys. Res. Lett.*, *39*, L13601, doi:10.1029/2012GL051963.

Dunne, J. P., R. A. Armstrong, A. Gnanadesikan, and J. L. Sarmiento (2005), Empirical and mechanistic models for the particle export ratio, *Global Biogeochem. Cycles*, *19*, GB4026, doi:10.1029/2004GB002390.

Dunne, J. P., J. L. Sarmiento, and A. Gnanadesikan (2007), A synthesis of global particle export from the surface ocean and cycling through the ocean interior and on the seafloor, *Global Biogeochem. Cycles*, *21*, GB4006, doi:10.1029/2006GB002907.

Friedland, K. D., C. Stock, K. F. Drinkwater, J. S. Link, R. T. Leaf, B. V. Shank, J. M. Rose, C. H. Pilskaln, and M. J. Fogarty (2012), Pathways between primary production and fisheries yields of large marine ecosystems, *PLoS One*, *7*(1), e28945.

Galbraith, E. D., et al. (2015), Complex functionality with minimal computation: Promise and pitfalls of reduced-tracer ocean biogeochemistry models, *J. Adv. Model. Earth Syst.*, *6*(1), 513–526.

Gillooly, J. F., J. H. Brown, G. B. West, V. M. Savage, and E. L. Charnov (2001), Effects of size and temperature on metabolic rate, *Science*, *293*, 2248–2251.

Henson, S. A., R. Sanders, E. Madsen, P. J. Morris, F. Le Moigne, and G. D. Quartly (2011), A reduced estimate of the strength of the ocean's biological carbon pump, *Geophys. Res. Lett.*, *38*, L04606, doi:10.1029/2011GL046735.

Henson, S. A., A. Yool, and R. Sanders (2015), Variability in efficiency of particulate organic carbon export: A model study, *Global Biogeochem. Cycles*, *29*, 33–45, doi:10.1002/2014GB004965.

Kass, R. E., and A. E. Raftery (1995), Bayes factors, *J. Am. Stat. Assoc.*, *90*(430), 773–795.

Kwon, E. Y., F. Primeau, and J. L. Sarmiento (2009), The impact of remineralization depth on the air–sea carbon balance, *Nat. Geosci.*, *2*(9), 630–635.

Laurenceau-Cornec, E. C., et al. (2015), The relative importance of phytoplankton aggregates and zooplankton fecal pellets to carbon export: insights from free-drifting sediment trap deployments in naturally iron-fertilised waters near the Kerguelen Plateau, *Biogeosciences*, *12*(4), 1007–1027.

Laws, E. A., E. D'Sa, and P. Naik (2011), Simple equations to estimate ratios of new or export production to total production from satellite-derived estimates of sea surface temperature and primary production, *Oceanogr. Methods*, *9*, 593–601.

Laws, E., P. G. Falkowski, W. O. Smith, H. Ducklow, and J. J. McCarthy (2000), Temperature effects on export production in the open ocean, *Global Biogeochem. Cycles*, *14*(4), 1231–1246, doi:10.1029/1999GB001229.

Lee, Z. P., A. Weidemann, J. Kindle, R. Arnone, K. L. Carder, and C. Davis (2007), Euphotic zone depth: Its derivation and implication to ocean-color remote sensing, *J. Geophys. Res.*, *112*, C03009, doi:10.1029/2006JC003802.

López-Urrutia, A., E. San Martin, R. P. Harris, and X. Irigoien (2006), Scaling the metabolic balance of the oceans, *Proc. Natl. Acad. Sci. U.S.A.*, *103*(23), 8739–8744.

Maiti, K., M. A. Charette, K. O. Buesseler, and M. Kahru (2013), An inverse relationship between production and export efficiency in the Southern Ocean, *Geophys. Res. Lett.*, *40*, 1557–1561, doi:10.1002/grl.50219.

Martin, P., et al. (2013), Iron fertilization enhanced net community production but not downward particle flux during the Southern Ocean iron fertilization experiment LOHAFEX, *Global Biogeochem. Cycles*, *27*, 871–881, doi:10.1002/gbc.20077.

Sarmiento, J. L., and N. Gruber (2013), *Ocean Biogeochemical Dynamics*, Princeton Univ. Press, Princeton, N. J.

Siegel, D. A., K. O. Buesseler, S. C. Doney, S. F. Sailley, M. J. Behrenfeld, and P. W. Boyd (2014), Global assessment of ocean carbon export by combining satellite observations and food-web models, *Global Biogeochem. Cycles*, *28*, 181–196, doi:10.1002/2013GB004743.

Siegel, D., et al. (2015), EXport Processing in the Ocean from RemoTe Sensing (EXPORTS): A science plan for a NASA field campaign, NASA, 1–101.

Teng, Y.-C., F. W. Primeau, J. K. Moore, M. W. Lomas, and A. C. Martiny (2014), Global-scale variations of the ratios of carbon to phosphorus in exported marine organic matter, *Nat. Geosci.*, *7*(1), 895–898.

Westberry, T., M. J. Behrenfeld, D. A. Siegel, and E. Boss (2008), Carbon-based primary productivity modeling with vertically resolved photoacclimation, *Global Biogeochem. Cycles*, *22*, GB2024, doi:10.1029/2007GB003078.